Influence of an Oriented Glassy Cylindrical Microdomain Structure on the Morphology of Crystallizing Lamellae in a Semicrystalline Block Terpolymer

Cheolmin Park,[†] Claudio De Rosa,[‡] Lewis J. Fetters,[§] and Edwin L. Thomas*[,†]

Department of Materials Science and Engineering, Program in Polymer Science and Technology, Massachusetts Institute of Technology, Cambridge, Massachusetts 02139; Dipartimento di Chimica, Universita' di Napoli "Federico II", Via Mezzocannone 4, 80134 Napoli, Italy; and Exxon-Mobil Research and Engineering Company, Corporate Strategic Research, Annandale, New Jersey 08801

Received May 4, 2000

ABSTRACT: The effect of an oriented microphase-separated structure, induced by an applied flow bias field (roll casting), on the crystallization of the polyethylene (PE) block in a semicrystalline polystyrene-*block*-(polyethylene-*alt*-propylene)-*block*-polyethylene terpolymer has been analyzed. The orientation and morphology of the emerging crystals with respect to the preexisting glassy cylindrical microdomain structure has been investigated by simultaneous wide-angle and small-angle X-ray scattering and transmission electron microscopy. The oriented hexagonally packed cylinders induce oriented crystallization of the PE block in the matrix upon slow cooling below the crystallization temperature. The texture which develops has the *b* and *c* axes of the PE crystals predominantly parallel and perpendicular to the PS cylinder axes, respectively. The lateral packing of the PS cylinders is disrupted by the crystallization, but the longitudinal orientation of the cylinders is maintained.

Introduction

Semicrystalline block copolymers have been studied for their possible application as replacements for glassy/rubbery block thermoplastic elastomers due to their improved mechanical properties as well as better thermal stability.[1−24] In addition, semicrystalline block copolymers have been recently shown to provide new means to nanoscale patterned thin films.[25−27] There exists strong scientific interest in these materials because they can undergo at least two thermodynamic transitions during their process history. Understanding how the competition of the crystallization, the microphase separation, and the glass transition leads to the final morphology is the key in furthering our knowledge of the properties of semicrystalline block copolymers.

In general, one can expect that the microstructure and physical properties of the material will be significantly influenced by the nature of the chain and domain organization in both the noncrystalline and crystalline blocks. The process pathway of structure formation is of prime importance in that the first forming structures present to those emerging a prescribed geometry into which the new structure must evolve. Studies have been done on anionically synthesized model block copolymers having a crystallizable block to reveal how the final sample morphology depends not only on the sequence of transitions the material experiences but also on the relative thermodynamic strengths of the transitions. Various groups[1−25] have shown that the morphology of semicrystalline block copolymers is path dependent; different microdomain structures are obtained if the crystallization occurs from a homogeneous melt (in this case the crystallization drives the microphase separation), or it occurs from an already microphase-separated heterogeneous melt. (In this case microphase separation precedes crystallization and provides a microstructure within which crystallization takes place.)

When the block incompatibility is small, as for instance for the block copolymers composed of crystallizable polyethylene (PE) blocks and poly(ethylene-*alt*-propylene) (PEP) or poly(ethylethylene) amorphous blocks, such as those analyzed by Rangarajan et al.,[6,9] crystallization occurs from a homogeneous melt, resulting in the formation of alternating lamellar microdomains in a spherulitic superstructure regardless of the copolymer composition,[5] as has been assumed in theoretical treatments.[28,29]

When the block segments have a larger interaction parameter and also have high molecular weights, microphase separation in the melt occurs prior to crystallization. The presence of microdomains in the ordered melt may affect the crystallization process and the final morphology.[1,2,4,7,8,14,17−19,21,24] However, when the order−disorder transition is close to the melting temperature of the crystallizable block, the energy barrier for destruction of the ordered melt is small, and the crystallization may alter the order achieved during the microphase separation. For example, a weakly segregated lamellar structure of the melt of ethylene/head-to-head propylene block copolymer was transformed into a strongly segregated spherulitic microstructure containing crystalline lamellae after crystallization of PE block.[9] A caprolactone−butadiene diblock copolymer[5] also clearly showed the replacement of the melt microstructure by a crystallization-driven morphology. Ryan et al.[11] showed that a cylindrical microstructure of the melt of poly(ethylene-*b*-ethylethylene) diblock copolymer is reorganized upon crystallization into a final spherulitic lamellar morphology.

In an AB diblock copolymer where the B block is crystallizable, the microdomain melt morphology can be

[†] Massachusetts Institute of Technology.
[‡] Universita' di Napoli "Federico II".
[§] Exxon-Mobil Research and Engineering Company.
* To whom correspondence should be addressed. Tel 617-253-6901; FAX 617-258-6135; e-mail elt@mit.edu.

10.1021/ma000772f CCC: $19.00
Published on Web 09/21/2000

preserved, when the T_g^A (the glass transition temperature of A block) > T_c^B (the crystallization temperature of B block). Such a situation confines the crystals to grow within or between the preexisting microseparated domains. Crystallization confined in preexisting lamellar,[4,7,8,14,21,24] spherical,[2] or cylindrical[1,17−20] microdomains has been observed.

Globally aligned semicrystalline block copolymers permit determination of the orientation of the crystals and the unit cell with respect to the microdomain interfaces. Cohen et al.[7,8] first used a channel die to orient PE containing semicrystalline block copolymers and showed that the chain axis of PE crystals is perpendicular to the normal direction of microphase-separated lamellar surfaces. Other workers also studied lamellar systems using the shear forces for alignment of the microphase-separated block copolymer structures and found that the orientation of the chain axis of crystals depends on several factors such as molecular weight of the block copolymer and the crystallization conditions.[14,15,24] Quiram et al.[20] recently used a channel die to study the crystal orientation in a sample wherein the crystallizable block constituted the cylindrical microdomains and demonstrated that the crystalline PE lamellae grow along the PE cylinder axis.

Studies of the oriented microstructure in the case that the crystallizable component forms and aligns within the majority matrix phase due to the preexisting minority glassy microstructure are not yet reported in single block copolymer system. Liu et al. showed that the crystalline poly(tetrahydofuran) (PTHF) block is oriented due to the confinement between the cylindrical poly(methyl methacrylate) (PMMA) microdomains in the blend of the diblock copolymer and homo PTHF.[30] However, they did not provide direct evidence of the molecular chain orientation.

In this paper we use simultaneous wide-angle X-ray scattering (WAXS), small-angle X-ray scattering (SAXS), and transmission electron microscopy (TEM) to study the morphology of a polystyrene-*block*-(polyethylene-*alt*-propylene)-*block*-polyethylene terpolymer (PS/PEP/PE). Since the PEP and PE blocks are completely miscible above the melting temperature (T_m) of PE,[23] a microstructure of PS microdomains in a matrix of mixed PE and PEP blocks is expected above the T_m of the PE component. When the temperature drops below the crystallization temperature of PE, another phase separation takes place within the matrix, due to the crystallization of PE. The PS and PE end-blocks are connected via the rubbery PEP mid-block, presenting a novel situation in which the crystallization of the PE end-block between the microphase-separated glassy PS structure is partially screened by the rubbery mid-block. To study the influence of the presence of well-aligned minority PS microdomains on the growth and organization of the PE molecular chains and PE crystalline lamellae, we employ the roll cast method at temperature above the crystallizing point of the PE and well below the microphase separation temperature to obtain an aligned hexagonally packed PS cylindrical microdomain structure.[31−33] The development of oriented crystalline PE microdomains was observed upon slow cooling in the well-defined microseparated PS structure by scattering and microscopy.

Experimental Methods

The polymer used was derived by hydrogenation of a polystyrene-*block*-polyisoprene-*block*-polybutadiene (PS/PI/PB) terpolymer synthesized at Exxon Research Co. The PS/PI/PB triblock was prepared by anionic polymerization in benzene at 20 °C with *sec*-BuLi as the initiator. The polymerization was done in a sequential fashion commencing with styrene. Conventional high-vacuum techniques were used.[34] The resultant PI microstructure yielded, after hydrogenation, the essentially alternating copolymer of ethylene and propylene while the PB segment yielded a poly(ethylene-*co*-butene) copolymer having approximately two ethyl branches per 100 backbone carbons. The hydrogenation was carried out using the procedures give elsewhere.[35−38] The method used leads to complete saturation of the polydiene segments while leaving the polystyrene segment unchanged.

Polymer molecular weight characterization was done using a combination of size exclusion chromatography (SEC) and low-angle laser light scattering. Tetrahydrofuran was the solvent in both cases. The weight-average molecular weight M_w of PS/PI/PB via light scattering was 103 000 g/mol, while SEC gave M_z/M_w and M_w/M_n ratios as 1.02 and 1.04, respectively. The molecular weights of the PS, PI, and PB blocks are 15 000, 70 000, and 15 000 g/mol, respectively. The calculated volume fractions of the PS block are 0.13 and 0.15 at 150 and 50 °C, respectively.

Anisotropic thick films (1 mm thickness) were made by pouring the polymer solution (15 wt % in decalin) between two temperature-controlled counterrotating adjacent cylinders while at the same time the solvent was allowed to evaporate. The angular velocity of each cylinder was about 30 rpm. The flow direction corresponds to *X*, the neutral direction to *Y*, and the through thickness direction to *Z*. The roll casting process was performed at the elevated temperature (90 °C) to avoid any effects of the crystallization of the PE block (which occurs at 70 °C) on the structure. Roll cast films were subsequently quenched in liquid N_2 to preserve the oriented PS microstructure formed above the crystallization temperature of PE[23] and dried in a vacuum oven at 40 °C for 24 h in order to remove all traces of the solvent. They were then annealed for an additional 10 days under vacuum at 140 °C, significantly above both the glass transition temperature of polystyrene segments ($T_g \sim 80$ °C) and the melting temperature of polyethylene segments. The films were then subsequently slowly cooled to room temperature with a cooling rate of 2 °C/min.

Thin sections of the roll cast films were prepared using a Reichert-Jung FC4E Ultracut microtome at −110 °C. Some samples were subsequently stained for 20 min with RuO_4, a preferential stain for the PS block. Bright-field TEM was then performed for both stained and unstained samples with a JEOL 200 CX microscope operated at 200 kV.

Simultaneous WAXS and SAXS measurements were also carried out at the Advanced Polymers Beamline, X27C, National Synchrotron Light Source, Brookhaven National Laboratory. The wavelength used was $\lambda = 0.1307$ nm, and the beam size was about 0.4 mm in diameter at the sample position. A three 2° tapered tantalum pinhole collimation system was utilized with a sample-to-detector distance of 1560 and 108 mm for SAXS and WAXS patterns, respectively. Scattering angles 2θ down to 1.5 mrad corresponding to a Bragg spacing ($d = 2\pi/q$ where $q = 4\pi \sin \theta/\lambda$) of about 100 nm were achieved. A single-cell heating stage (maximum temperature: 350 °C) was used for high-temperature measurements. Fuji imaging plates were used to collect the scattering data with exposure times of 1 min per frame.

The melting temperatures and the crystallinity indices were obtained with calorimetric measurements using a differential scanning calorimeter Perkin-Elmer DSC-7, performing scans in a flowing N_2 atmosphere at a heating rate of 2 °C/min. The crystallinity indices was calculated from the values of the experimental melting enthalpy and the value of the equilibrium melting enthalpy of a perfect crystal of PE (289 J/g).[39] The melting temperature of both the quenched and the slowly cooled roll cast samples was 98 °C, significantly lower than that of high-density polyethylene, indicative of the presence of the ethyl branches. The crystallinity index of both samples was about 40% with respect to the crystallizable PE block,

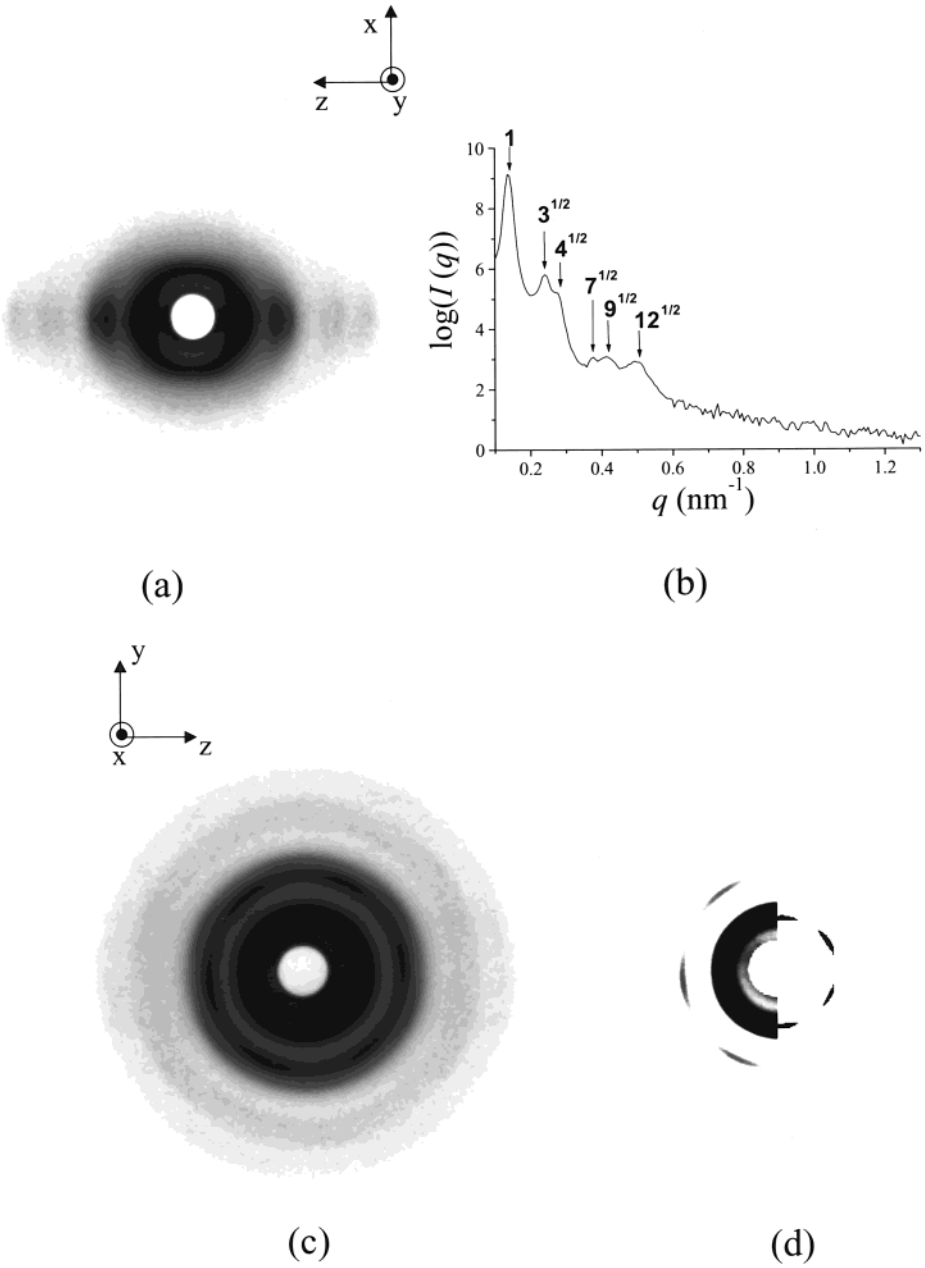

Figure 1. (a) 2-dimensional SAXS pattern of the roll cast sample taken at 150 °C with the incident beam perpendicular to the flow direction, normal to the *XZ* plane. Several strong reflections are shown perpendicular to the flow direction. (b) SAXS profile along the horizontal (equatorial) direction of (a) shows peaks in the ratio of 1:√3:√4:√7:√9:√12, etc., implying the structure is characterized by a hexagonal packing of cylinders. (c) 2-dimensional SAXS pattern of the roll cast sample at 150 °C with the incident beam along the flow direction, normal to the *YZ* plane. (d) SAXS pattern with different threshold cutoff to emphasize the 6-fold symmetry of the first- and second-order reflection.

corresponding to only 6% with respect to the total weight of the block copolymer.

Results and Discussion

Figure 1a shows the SAXS pattern of a roll cast sample after long-term annealing, heated to 150 °C with the incident beam normal to the *XZ* plane, perpendicular to the flow direction. The scattering is concentrated along the normal to the flow direction. The intensity scan across the equator as a function of the scattering vector is shown in Figure 1b. The set of Bragg peaks present in Figure 1a have q_n/q_1 approximate values of 1.0, √3, √4, √7, √9, etc. (where q_1 is the scattering vector of the first peak $q_1 = 0.14$ nm^{-1}), which corresponds well with a hexagonal packing. Figure 1c shows the SAXS pattern of the roll cast film recorded with the incident X-ray beam along the normal to the *YZ* plane, parallel to the flow direction. Adjusting the threshold cutoff intensity allows emphasis of the 6-fold symmetry of both the first- and second-order reflection in Figure 1d. As expected, the pattern presents an approximate 6-fold symmetric set of intense reflections, which indicates that the roll casting process has induced a well-oriented, highly ordered structure. SAXS therefore indicates that the structure is a two-dimensionally ordered hexagonal packing of PS cylinders whose axes are parallel to the flow direction. The value of the scattering vector of the first peak ($q_1 = 0.14$ nm^{-1}), corresponding to the $(10\bar{1}0)$ reflection, indicates that the hexagonal lattice has a periodicity of 45 nm. The 150 °C SAXS patterns for the two different incident beam directions are very similar to those of the quenched roll

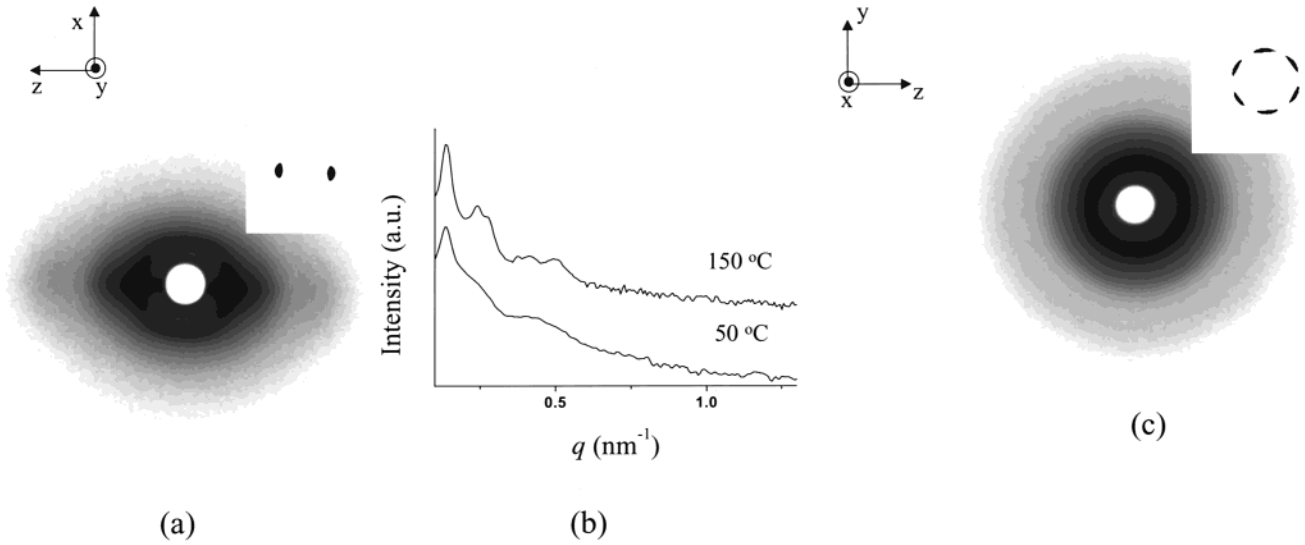

Figure 2. (a) 2D SAXS pattern of the slowly cooled sample taken at 50 °C when the incident beam perpendicular to the *XZ* plane. The pattern with a different threshold cutoff to emphasize the first-order reflection is shown in the inset. It confirms that the oriented structure of the PS microdomains formed by the applied flow field is preserved after the crystallization of PE. (b) Comparison between the SAXS profiles along the horizontal (equatorial) direction (±10° sector slice) at 150 and at 50 °C. The increase of the scattering intensity at the high q region ($q = 0.4-0.5$ nm^{-1}), due to the presence of the crystalline PE lamellae is apparent in the 50 °C pattern. (c) 2D SAXS pattern of the slowly cooled sample at 50 °C when the incident beam along the flow direction normal to *YZ* plane. The same pattern with a different threshold cutoff to emphasize the 6-fold symmetry of the first $\sqrt{1}$ reflection is shown in the inset. The $\sqrt{3}$ reflection is only observed as a weak, broad continuous ring. It indicates that the lateral packing of the PS microdomain structure developed during the roll cast was perturbed by the crystallization of PE.

cast sample investigated in our previous paper.[23] Since the small PE crystals developed during the quenching step do not disturb the cylindrical PS microdomain structure, the microstructure at room temperature after quenching can be assumed the same as that at 150 °C.[23] The TEM micrographs of the quenched samples in our previous work suggest that the microstructure at 150 °C is a hexagonally packed cylinder structure as expected from the SAXS results. However, the PS cylinders are not the customary infinitely long straight units. Rather, they display a range of prolate structures aligned along the flow direction. Many defect points along the cylinder axis occur due to low volume fraction of the PS block (0.13) as well as due to high activation energy to reach the equilibrium cylindrical microstructure.[23]

The SAXS patterns, recorded during the cooling with the rate of 2 °C/min, do not change much with decreasing temperature until around 70 °C. At this temperature the first- and higher-order peaks broaden, and a shoulder appears at the high q region. The patterns become diffuse above $q = 0.2$ nm^{-1}, indicating disturbance of the microdomain pattern by the PE crystals and the superposition of peaks arising from the interlamellae scattering of the crystalline PE regions in the matrix. A similar thermal treatment of the hydrogenated 1,4 PB homopolymer with a molecular weight of 65 000 g/mol and the same butyl content ratio give a first-order reflection peak around $q \sim 0.2$ nm^{-1} and a broad intermediate peak ($q \sim 0.4$ nm^{-1}) (data not shown).

Figure 2 shows the SAXS patterns of the slowly cooled sample at 50 °C, when the incident beam is perpendicular to the *XZ* (a) and *YZ* planes (c). The intensity scan across the equator of the block copolymer melt, recorded at 50 °C, is compared to that for 150 °C in Figure 2b. The increased intensity around $q \sim 0.2$ nm^{-1} and broad scattering intensity at $q \sim 0.4-0.5$ nm^{-1}, in the pattern at 50 °C, are due to scattering from the crystalline PE lamellae and/or due to the partial distortion of the preexisting microstructure (Figure 2b). The invariant location of the first peak at $q = 0.14$ nm^{-1} (compare with the pattern at 150 °C), and the retention of the 2-fold and the 6-fold symmetry axes, clearly shown in the insets of parts a and c of Figure 2, respectively, indicate that the texture developed during the roll cast process remains after crystallization. The SAXS patterns indicate that the axes of PS cylinders are still parallel to the flow direction and the average distance between the hexagonally packed cylinders is still 48 nm. The distortion of the microstructure due to the crystallization of the PE primarily affects the intercylinder lateral packing, resulting in the loss of the higher-order reflections.

The effect of the PE crystallization on the orientation of the cylindrical PS microdomains along the flow direction can be made by comparing the full width half-maximum (fwhm) values at 50 °C to those at 150 °C. The azimuthal scattered intensity distributions of the $(10\bar{1}0)$ reflection at 50 and 150 °C of Figures 2a and 1a, respectively, are shown in Figure 3. Both azimuthal fwhm are approximately 45°, indicating that the orientation of the cylindrical PS microdomains does not change along the flow direction due to crystallization of the PE component.

The WAXS pattern of the slowly cooled sample recorded at 50 °C with the incident beam normal to the *XZ* plane is shown in Figure 4a. The pattern presents four evident rings: an unoriented, broad innermost ring due to scattering from amorphous PS, PEP, and PE regions and three oriented, narrow, outer rings corresponding to the (110), (200), and (020) reflections arising from the PE crystals in the usual orthorhombic form. It is apparent that the (110) reflection is textured into four off-axis regions of high intensity, while the less intense (200) and (020) reflections show two arcs concentrated on the equator and on the meridian, respectively. A schematic of the WAXS pattern is given in Figure 4b. The presence of four arcs for the 110

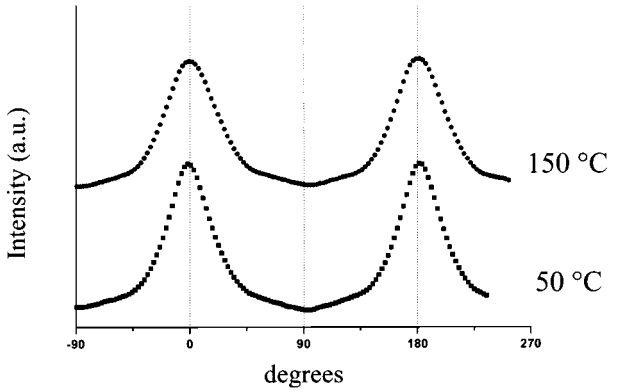

Figure 3. Equatorial azimuthal intensity distribution profiles of the (10$\bar{1}$0) reflection at 150 °C in Figure 1a and at 50 °C in Figure 2a. Two highly oriented peaks appear at 0° and 180° at both temperatures. The fwhm value of the peak is approximately 45° in both cases, indicating that the crystallization of the PE block does not disturb the orientation of the cylindrical PS microdomains along the flow direction.

reflection, two equatorial arcs for the (200) reflections, and two meridian arcs for (020) indicates that the PE lamellae are oriented with the *b* axis parallel to the flow direction. The SAXS (Figure 2a) and WAXS (Figure 4a) patterns, therefore, suggest that the crystalline PE lamellae are primarily oriented with their *b* axis parallel, and the chain axis normal, to the axes of the PS cylinders. The measure of azimuthal separation of the (110) reflection peaks is approximately 114°, which indicates within experimental uncertainty that the PE crystal stems are preferentially oriented perpendicular to the PS cylinder axis.[20] The WAXS pattern with the incident X-ray beam directed along the *X* axis, parallel to the flow direction, and therefore parallel to the *b* axis, reported in Figure 4c, displays isotropic rings for the (110) and (200) reflection. Although the 6-fold symmetry of the oriented $\sqrt{1}$ reflection of the cylindrical PS microdomain structure is still evident after the PE crystallization (Figure 2c), the PE crystals formed between the PS cylinders show ∞-fold rotational symmetry of their *b* axes around the PS cylinder axis. Strong crystallization forces disturb the long-range lateral packing of the PS cylinders as described earlier.

The axial orientation of the PE crystals can be also assessed by the fwhm of the (020) reflection of Figure 4a. The fwhm value corresponds to the degree of the orientation of the *b* axis of the PE crystals along the flow direction. The value is about 45°, which is consistent with the degree of the orientation of the PS cylinders along the flow direction measured by the azimuthal fwhm of the (10$\bar{1}$0) reflection at 50 °C in Figure 3 (∼45°). An approximately axisymmetric orientation of the PE lamellae around the *b* axis, which is parallel to the PS cylinder axis, accounts for WAXS patterns of Figure 4.

When cooled below T_c^{PE}, crystalline PE lamellae nucleate and grow in various directions. The fast growth direction of the PE crystals is the *b* axis direction.[40] In the present work, when the fast growth direction of the crystalline PE lamellae is parallel to the cylinder axis of the PS microdomains, large crystals can grow, whereas in other directions, the crystals encounter the PS microdomains. This bias results in the preferred alignment of the *b* axis of the PE parallel to the PS cylinder axis.

TEM of the RuO_4 stained sections permits direct visualization of the PS cylinders in the slowly cooled sample. A transverse view of the PS cylinders parallel to the flow field is observed in Figure 5a. The PS

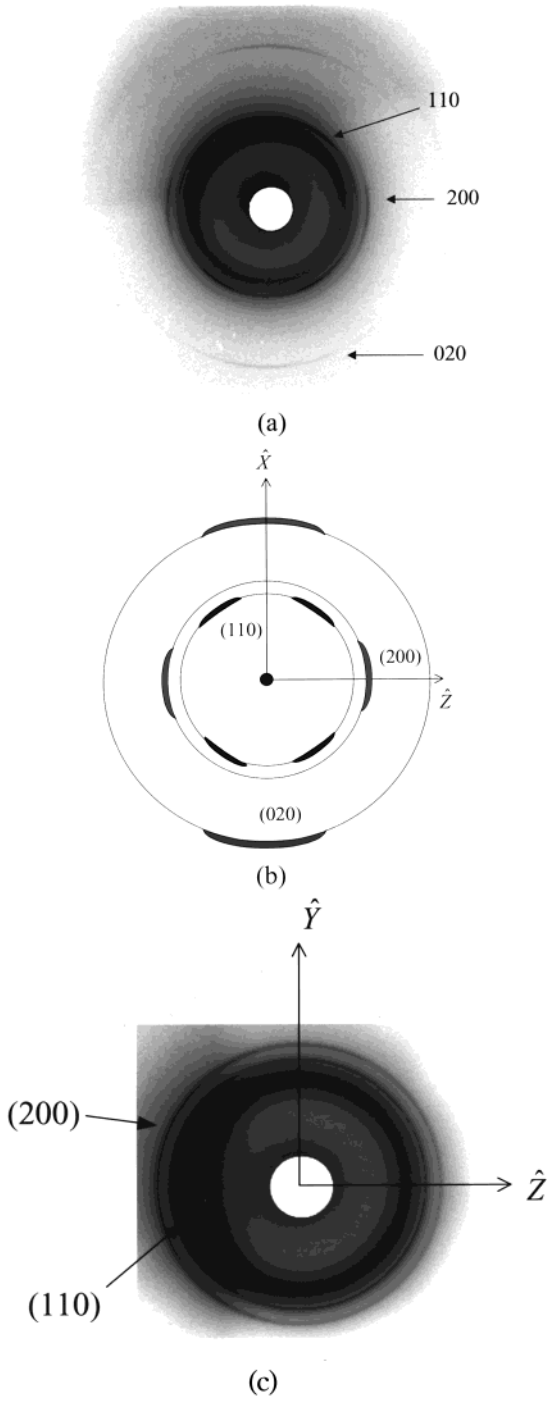

Figure 4. (a) 2-dimensional WAXS patterns, obtained simultaneously with the SAXS pattern of Figure 2a, of the slowly cooled sample with the incident beam normal to the *XZ* plane. The diffuse inner ring is the unoriented amorphous halo. The first crystalline reflection corresponds to (110) reflection of orthorhombic PE crystals and displays four off-axis regions of high intensity. The (200) and (020) reflections are preferentially located on the equator and on the meridian, respectively. These features indicate that the PE lamellae are oriented with the *b* axis normal to the X-ray beam and therefore parallel to the flow direction. (b) Schematic diagram of the WAXS pattern with indexed reflections. (c) 2-dimensional WAXS pattern, obtained simultaneously with SAXS pattern of Figure 2c, of the slowly cooled sample with the incident beam normal to the *YZ* plane. The isotropic (110) and (200) diffraction rings indicate uniaxial symmetry around the *b* axis of the PE crystals.

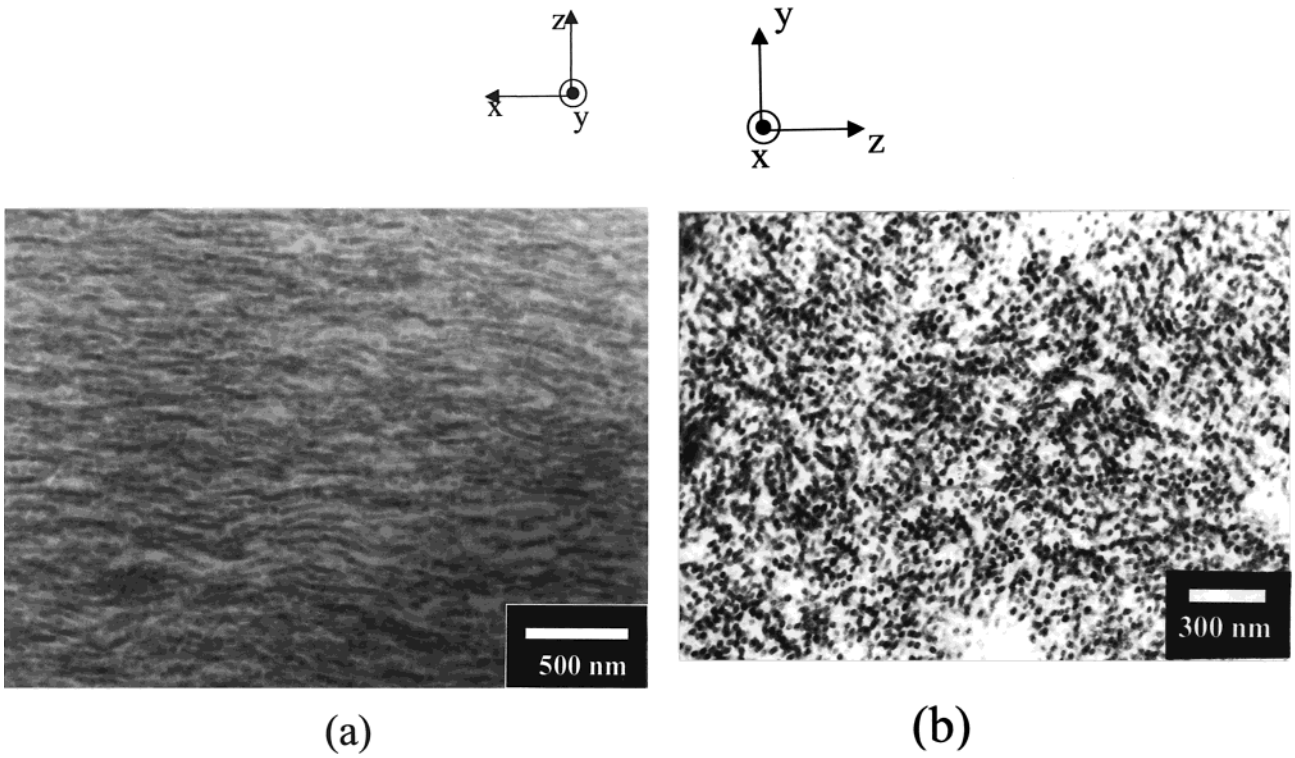

Figure 5. Bright field TEM images of the microtomed sections of the slowly cooled roll cast films stained with RuO_4. (a) Transverse view showing PS cylinders aligned parallel to the flow direction. The orientation of PS cylinders is still preserved after the crystallization of PE. (b) Axial view showing circular cross sections of PS cylinders. The hexagonally packed structure, observed in the SAXS pattern taken at 150 °C, is disrupted by the crystallization of PE in the matrix.

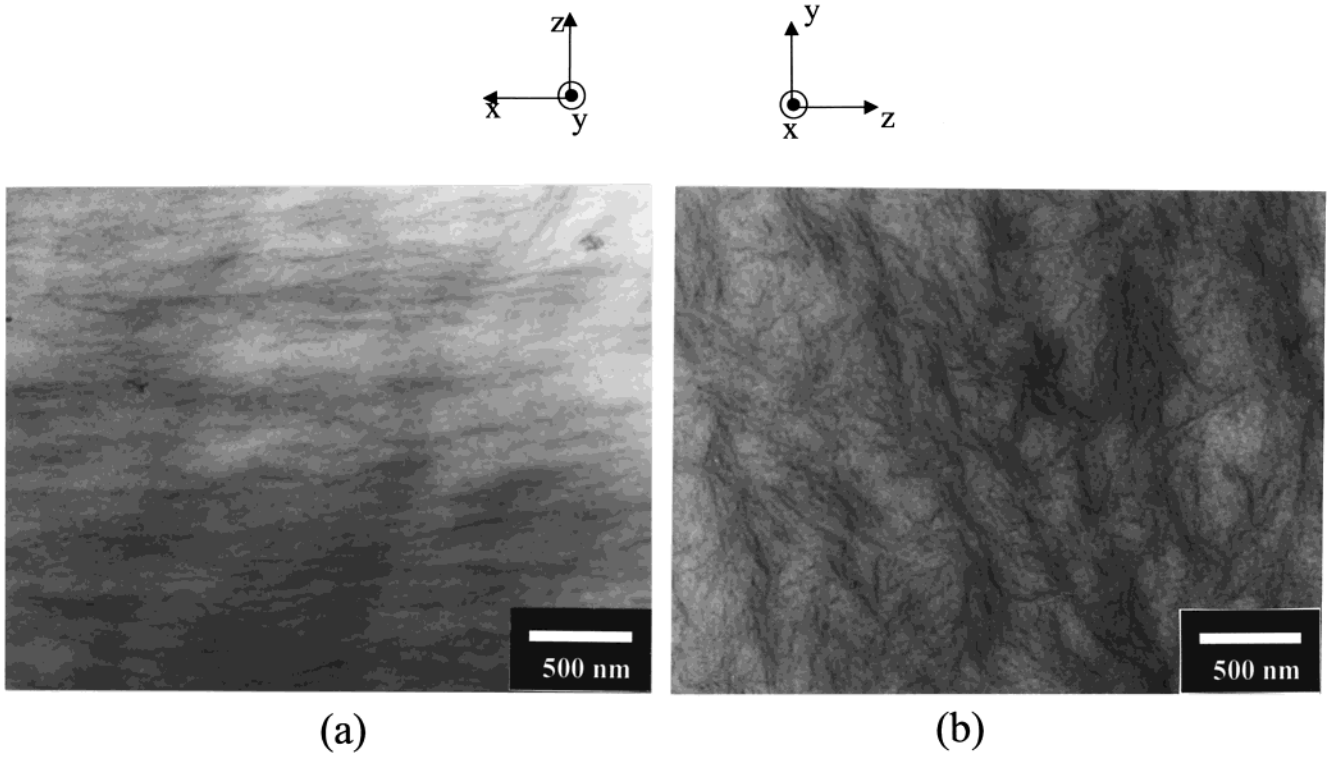

Figure 6. Underfocus phase contrast bright field TEM images of the microtomed sections of the unstained roll cast films slowly cooled to room temperature. (a) Transverse view showing crystalline PE lamellae (seen edge-on) (dark region), oriented along the roll casting direction. The thickness of lamellae ranges from 10 to 20 nm. (b) Axial view showing crystalline PE lamellae (seen edge-on) oriented in various directions.

cylinders display waviness and a distribution of lengths. The average diameter of the PS cylindrical microdomains is nearly 20 nm, and the average distance between the cylinders is 40−50 nm, in agreement with the SAXS data. The oriented structure along the flow direction in Figure 5a is very similar to that of the quenched sample in our previous work.[23] The crystallization of the PE block does not much affect the preoriented PS microstructure along the flow direction consistent with the fwhm data (Figure 3). However, the

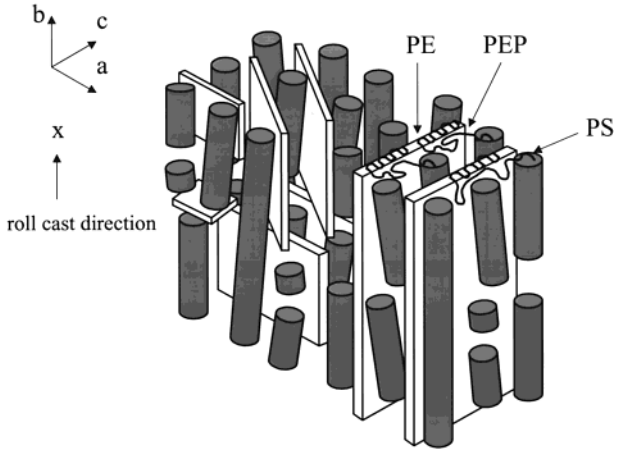

Figure 7. Schematic diagram of the microdomain structure of the slowly cooled roll cast sample. The crystallization of PE is confined between the preformed hexagonally packed PS cylinders, and *b* and *c* axes of the PE crystals are preferentially parallel and perpendicular to the axes of the PS cylinders, respectively. Various orientations of the crystalline PE lamellae develop on the view of the *YZ* plane not only due to the hexagonal symmetry of the cylindrical PS microdomains but also due to many defects and misaligned PS cylinders in the roll cast microstructure. In addition, random nucleation of the PE crystals in the matrix generates various other orientations.

hexagonally packed structure is disturbed by the crystallization of PE in the matrix as evident from Figure 5b. The axial view of the structure shows circular cross sections of the RuO_4 stained PS cylinders with poor lateral registry. In comparison with Figure 4a of ref 23, the crystallization of the PE lamellae via the slow cooling significantly disrupts the hexagonal packing of the PS cylinders.

The crystalline PE lamellae can be seen in the TEM micrographs of the unstained sample as reported in Figure 6a,b. Phase contrast obtained by underfocus of the objective lens makes the noncrystalline regions appear bright.[41] The phase contrast is proportional to the mean inner potential difference between microdomains projected through the specimen. The mean inner potentials of the blocks in the terpolymer are 7.35, 7.08, and ≈6.3 for the PE crystal, the PS, and amorphous PE and PEP, respectively.[41] Thus, those lamellae that are oriented edge-on to the electron beam direction and completely traverse the sample provide the highest contrast. For the regions where the projection across the sample includes the PS, PEP, and PE domains, the contrast is much lower and does not uniquely correspond to domain size. When viewed along the normal to the *XZ* plane (Figure 6a), those crystalline PE lamellae for which the *b* axis is parallel to the PS cylinders are evident. The thickness of lamellae is estimated as 10−20 nm. In the TEM image viewed along the flow direction, i.e., along the axes of the PS cylinders and the *b* axis of the PE lamellae, the crystalline PE lamellae are seen edge-on oriented in various directions (Figure 6b). The TEM images confirm that the PE lamellae are oriented with their *b* axes parallel to the axes of the PS cylinders but have many orientations around the *b* axis.

A model of the PS−PEP−PE terpolymer microstructure after the crystallization of the PE block is shown in Figure 7. The crystallization of PE is confined between the preexisting pseudohexagonally packed PS cylinders. The PE chain axis is preferentially oriented orthogonal to the PS cylinder axis with the fast growth *b* axis direction of PE parallel to the axis of the cylinders. This type of unit cell orientation occurs because it allows the PE lamellae to grow long in the direction parallel to the PS cylinders. This orientation was also observed by Quiram et al.[20] in the case of a poly(ethylene-*b*-vinylcyclohexane) where the crystallization occurred within the cylindrical PE microdomains. Rotation of crystalline lamellae around the average cylinder axis direction may occur when the growing lamellae encounter some defects such as, for instance, misaligned PS cylinders and prolate PS spheres as shown in TEM micrographs of Figure 5a. The development of lamellae with different orientations results in the partial disturbance of the long-range hexagonal packing of the PS cylinders. In an ideal hexagonal packing microstructure, three different orientations of the planar crystalline lamellae on the view of the *YZ* plane could be expected. However, in our sample, the initial roll cast structure is not perfect in terms of cylinder packing, orientation, and defects. Also, the random nucleation of the PE crystals results in a variety of lamellar orientations with the strong forces of crystallization tending to disrupt the lateral packing of the PS microdomains. Those crystallizing lamellae, which have their *b* axes parallel to the PS cylinder axis, develop preferentially, leading to an overall orientation of the PE *b* axis.

Conclusions

The crystallization of PE component in the matrix of the semicrystalline PS/PEP/PE block terpolymer does not significantly disturb the orientation of the preexisting cylindrical PS microdomain structure but does disrupt the lateral packing of the PS cylinders. The oriented microstructure of the minority PS phase induces orientation of the crystallizing PE microdomains. Crystalline PE lamellae organize themselves with the fast growth direction of the PE following the orientation of the PS cylinders. The strong forces of crystallization disrupt the lateral packing of the PS cylinders. The *b* and *c* axes of the PE crystals are predominantly parallel and perpendicular to the axes of the PS cylinders, respectively.

A preformed oriented microstructure is shown to be able to induce orientation of the subsequent lamellae crystallizing in the matrix. Furthermore, this study, using the model semicrystalline block terpolymer, provides a way to control the morphology of the nanocomposite of semicrystalline polymer and fillers (organic and inorganic types). Prealigned nanoscale anisotropic fillers such as nanotube and clays could induce the orientation of the crystalline phase of the semicrystalline polymer matrix.

Acknowledgment. This research is supported by the National Science Foundation DMR98-07591and also ACS PRF-300350-AC7. We gratefully acknowledge Dr. Y. Zhang, Mr. C. Osuji, Dr. F. Yeh, and Prof. B. Hsiao for their help at beamline X27C at Brookhaven National Laboratory. We are grateful to Mr. A. Eisen for valuable comments in roll cast film preparation. We thank the MIT Center for Materials Science and Engineering for the use of its TEM facility.

References and Notes

(1) Seguela, R.; Prud'homme, J. *Polymer* **1989**, *30*, 1446.

(2) Cohen, R. E.; Cheng, P. L.; Douzinas, K.; Kofinas, P.; Berney, C. V. *Macromolecules* **1990**, *23*, 324.
(3) Douzinas, K. C.; Cohen, R. E.; Halasa, A. F. *Macromolecules* **1991**, *24*, 4457.
(4) Douzinas, K. C.; Cohen, R. E. *Macromolecules* **1992**, *25*, 5030.
(5) Nojima, S.; Kato, K.; Yamamoto, S.; Ashida, T. *Macromolecules* **1992**, *25*, 2237.
(6) Rangarajan, P.; Register, R. A.; Fetters, L. J. *Macromolecules* **1993**, *26*, 4640.
(7) Cohen, R. E.; Bellare, A.; Drzewinski, M. A. *Macromolecules* **1994**, *27*, 2321.
(8) Kofinas, P.; Cohen, R. E. *Macromolecules* **1994**, *27*, 3002.
(9) Rangarajan, P.; Register, R. A.; Adamson, D. H.; Fetters, L. J.; Bras, W.; Naylor, S.; Ryan, A. J. *Macromolecules* **1995**, *28*, 1422.
(10) Rangarajan, P.; Register, R. A.; Fetters, L. J.; Bras, W.; Naylor, S.; Ryan, A. J. *Macromolecules* **1995**, *28*, 4932.
(11) Ryan, A. J.; Hamley, I. W.; Bras, W.; Bates, F. S. *Macromolecules* **1995**, *28*, 3860.
(12) Yang, Y.-W.; Tanodekaew, S.; Mai, S.-M.; Booth, C.; Ryan, A. J.; Bras, W.; Viras, K. *Macromolecules* **1995**, *28*, 6029.
(13) Khandpur, A. K.; Macosko, C. W.; Bates, F. S. *J. Polym. Sci., Polym. Phys. Ed.* **1995**, *33*, 247.
(14) Hamley, I. W.; Fairclough, J. P. A.; Terril, N. J.; Ryan, A. J.; Lipic, P. M.; Bates, F. S.; Town-Andrews, E. *Macromolecules* **1996**, *29*, 8835.
(15) Hamley, I. W.; Fairclough, J. P. A.; Ryan, A. J.; Bates, F. S.; Town-Andrews, E. *Polymer* **1996**, *37*, 4425.
(16) Ryan, A. J.; Fairclough, J. P. A.; Hamley, I. W.; Mai, S.-M.; Booth, C. *Macromolecules* **1997**, *30*, 1723.
(17) Rangarajan, P.; Haisch, C. F.; Register, R. A.; Adamson, D. H.; Fetters, L. J. *Macromolecules* **1997**, *30*, 494.
(18) Quiram, D. J.; Register, R. A.; Marchand, G. R. *Macromolecules* **1997**, *30*, 4551.
(19) Quiram, D. J.; Register, R. A.; Marchand, G. R.; Ryan, A. J. *Macromolecules* **1997**, *30*, 8338.
(20) Quiram, D. J.; Register, R. A.; Marchand, G. R.; Adamson, D. H. *Macromolecules* **1998**, *31*, 4891.
(21) Hillmyer, M. A.; Bates, F. S. *Macromol. Symp.* **1997**, *117*, 121.
(22) Balsamo, V.; von Gyldenfeldt, F.; Stadler, R. *Macromol. Chem. Phys.* **1996**, *197*, 3317.
(23) Park, C.; Simmons, S.; Fetters, L. J.; Hsiao, B.; Yeh, F.; Thomas, E. L. *Polymer* **2000**, *41*, 2971.
(24) Zhu, L.; Cheng, S. Z. D.; Calhoun, B. H.; Ge, Q.; Quirk, R. P.; Thomas, E. L.; Hsiao, B. S.; Yeh, F. *J. Am. Chem. Soc.* **2000**, *122*, 5957.
(25) De Rosa, C.; Park, C.; Thomas, E. L.; Lotz, B. *Nature* **2000**, *405*, 433.
(26) De Rosa, C.; Park, C.; Lotz, B.; Wittmann, J.; Fetters, L. J.; Thomas, E. L. *Macromolecules* **2000**, *33*, 4871.
(27) Reiter, G.; Castelein, G.; Hoerner, P.; Riess, G.; Blumen, A.; Sommer, J. U. *Phys. Rev. Lett.* **1999**, *83*, 3844.
(28) Di Marzo, E. A.; Guttman, C. M.; Hoffman, J. D. *Macromolecules* **1980**, *13*, 1194.
(29) Whitmore, M. D.; Noolandi, J. *Macromolecules* **1988**, *21*, 1482.
(30) Liu, L.; Chu, B. *J. Polym. Sci., Part B: Polym. Phys.* **1999**, *37*, 779.
(31) Albalak, R. J.; Thomas, E. L. *J. Polym. Sci., Part B: Polym. Phys.* **1993**, *32*, 37.
(32) Albalak, R. J.; Thomas, E. L. *J. Polym. Sci., Part B: Polym. Phys.* **1994**, *32*, 341.
(33) Albalak, R. J.; Thomas, E. L.; Capel, M. S. *Polymer* **1997**, *38*, 3819.
(34) Morton, M.; Fetters, L. J. *Rubber Chem. Technol.* **1975**, *48*, 359.
(35) Falk, J. C.; Schlott, R. J. *Macromolecules* **1971**, *4*, 152.
(36) Falk, J. C.; Schlott, R. J. *Angew. Makromol. Chem.* **1972**, *21*, 17.
(37) Falk, J. C. *Makromol. Chem.* **1972**, *160*, 291.
(38) Falk, J. C.; Fleet, J. V. *Macromol. Synth.* **1985**, *9*, 41.
(39) Wunderlich, B. *Macromolecular Physics*; Academic Press: New York, 1973; Vol. 1, Chapter 4.
(40) Keith, H. D.; Padden, F. J.; Vadimsky, R. G. *J. Polym. Sci.* **1966**, *4*, 267.
(41) Handlin, D. L.; Thomas, E. L. *Macromolecules* **1983**, *16*, 1514.

MA000772F